J. Electrochem. Sci. Eng. **15(1)** (2024) 2532; http://dx.doi.org/10.5599/jese.2532

Open Access : : ISSN 1847-9286
https://pub.iapchem.org/ojs/index.php/JESE

Original scientific paper

Exploring the impact of Al-based electrolytes on the charge storage behaviour of vine shoots derived carbon

Jana Mišurović[1,✉], Aleksandra Gezović Miljanić[1], Veselinka Grudić[1], Robert Dominko[2], Milica Vujković[3,4]

[1]*University of Montenegro - Faculty of Metallurgy and Technology, Cetinjski put bb, 81000 Podgorica, Montenegro*

[2]*National Institute of Chemistry, Hajdrihova 19, SI-1000, Ljubljana, Slovenia*

[3]*University of Belgrade - Faculty of Physical Chemistry, Studentski trg 12-16, 11158 Belgrade, Serbia*

[4]*Center for Interdisciplinary and Multidisciplinary Studies, University of Montenegro, Podgorica, Montenegro*

Corresponding author: ✉*janam@ucg.ac.me*

Received: October 15, 2024; Accepted: November 30, 2024; Published: December 11, 2024

Abstract

A new concept for affordable supercapacitors based on Al aqueous electrolytes was proposed recently. This study provides a deeper insight into the cyclic performance of vine shoots-derived activated carbon using three different 1 M aqueous electrolytes: $Al_2(SO_4)_3$, $Al(NO_3)_3$ and $AlCl_3$. Cyclic voltammetry (CV), galvanostatic cycling and impedance measurements have shown that the type of anion causes the differences in the rate capability and long-term cyclability. Although CV deviation is provoked by aggravated sulphate penetration into pores upon switching at higher currents, $Al_2(SO_4)_3$ emerged as the most promising electrolyte solution due to the best cycling stability of the 1.5 V full cell over 15,000 cycles. Intensive oxidation of the positive electrode during initial cycling, induced by nitrates reduction, is the main reason for the fastest capacitance drop observed in $Al(NO_3)_3$. Therefore, the capacitance values of the carbon cell measured after 5,000 cycles in $Al(NO_3)_3$ (75 F g^{-1}) are two times lower than the corresponding values in $Al_2(SO_4)_3$ and $AlCl_3$ (131 and 127 F g^{-1}, respectively). The oxidation becomes more pronounced only after 10,000 cycles in $AlCl_3$, thus causing a notable capacitance drop, which is not evidenced in $Al_2(SO_4)_3$. $Al_2(SO_4)_3$-based cell can withstand 15,000 with good specific capacitance/energy retention.

Keywords

Al-based supercapacitors; aqueous electrolyte; cyclic stability aspect

Introduction

The viticulture industry produces large amounts of carbon-rich bio-waste and represents a valuable feedstock for the development of a broad material selection with many specific applications. Various byproducts of the grape processing lines have been investigated for different energy-related and environmental applications [1-6]. Vineyard pruning residues, vine shoots, make the most of the dry-basis waste, which takes up enormous space and is most often disposed of by incineration. To prevent the negative effects of this practice, new sustainable alternatives are required. Until now, vine shoot-derived carbons have been considered for the adsorption of different substances [7-10] and energy-related applications, including supercapacitors [11-13]. Especially, carbon derived from vine shoots emerged as a promising electrode for versatile aqueous-based supercapacitors [13].

In addition to the electrode material, the electrolyte significantly determines the overall performance of supercapacitor cell. Several advantages related to conductivity, viscosity, toxicity, and flammability push aqueous electrolytes before conventional organic ones. Nonetheless, thermodynamic limitations on workable voltage window (1.23 V) make them inferior to the organic electrolyte (≈2.7 V typically for acetonitrile or propylene carbonate mixed with an organic salts). Typical acidic (H_2SO_4) and alkaline (NaOH) aqueous electrolytes usually allow only a maximal operating voltage of 1 V.

The use of neutral salts based on sulphates (Li_2SO_4, K_2SO_4, Na_2SO_4) [14-17] and nitrates (typically $LiNO_3$) [18-20] stretches the potential window up to ≈ 2 V, with an operative voltage of 1.5 V delivering stable capacitance. Studying the mechanism of carbon-based supercapacitors in these electrolytes, Frackowiak *et al.* [18] concluded that Li_2SO_4 appeared to be the most promising electrolyte. More precisely, the interplay between variables, including the type of material, binder, current collector, hydrogen storage ability, ion solvent and ion-pore interaction, determines the final performance. For instance, the type of electrolyte anions (sulphates or nitrates) may cause the different hydrogen storage capabilities of the carbon and different redox processes occurring at the interface upon prolonged cycling to 1.8 V [18]. This leads to the higher initial energy/power density for $LiNO_3$-based supercapacitors but lower stability due to additional nitrate-related redox reactions.

Recently, acidic $Al_2(SO_4)_3$ was proposed as an additional approach capable of opening water boundaries beyond the thermodynamic stability window [13]. To the best of our knowledge, no comparative and detailed studies about using different Al-based aqueous electrolyte formulations for supercapacitors have been reported so far. Herein, three different Al-based electrolyte formulations were used to examine the performance of vine shoots-derived carbon. The role of anions (SO_4^{2-}, NO_3^-, Cl^-) on the performance and long-term stability of high voltage Al-based symmetric AC_{vs} supercapacitors was investigated.

Experimental

Material preparation

Activated carbon was obtained by the carbonization of winemaking industry waste, vine shoots, via a previously reported two-step route [13]. Vine shoots collected in the area near Podgorica, Montenegro, were washed, chopped, ground and dried in the air to be prepared for carbonization. First, the precursor was heated for 2 h at a lower temperature (300 °C) under Ar atmosphere with a heating rate of 5 °C min^{-1}. Second, the obtained material was mixed with $ZnCl_2$ in a mass ratio 1:3, respectively, and carbonized for another 2 h at 700 °C under Ar atmosphere (heating rate of

5 °C min^{-1}). The final product was thoroughly washed with 4 M HCl, hot distilled water, and cold distilled water to remove zinc residues and chlorides completely. In further text, the obtained carbon is designated $AC_{vs}700$.

Material characterization

XRD of $AC_{vs}700$ was measured on Rigaku MiniFlex600 X-ray diffractometer operating in para-focusing Brag-Brentano geometry. The source of X-ray Cu-Kα radiation was coupled to a D/teX Ultra2 MF semiconductor strip-type detector with direct detection. The operating conditions of the instrument were a voltage of 40 kV and a current of 15 mA. The sample was mounted on a Silica support and the diffractogram was recorded in the 10 to 80° 2θ angle range, with a step of 0.01°, at a data acquisition rate of 10.00°/min.

SEM micrographs were obtained using SEM FEI Scios2 dual beam system.

Electrochemical methods

Cyclic voltammetry (CV) was performed by using Gamry 1010E Potentiostat/Galvanostat in a typical three-electrode configuration, where saturated calomel electrode (SCE) and platinum foil served as reference and counter electrodes, respectively. The working electrode was a glassy carbon rod with active material ($AC_{vs}700$) slurry distributed evenly on its surface. For all measurements, the slurry was prepared by mixing the active material with a binder (5 wt.% Nafion in ethanol/water = = 95/5 weight ratio, Sigma Aldrich) in the mass ratio 95 : 5 and adding the appropriate amount of ethanol to form a viscous mixture. It was further treated ultrasonically until the desired flow was obtained and transferred to a glassy carbon surface in a very thin layer (mass loading was kept at ≈1 to 1.5 mg cm^{-2}). CV measurements were performed at different scan rates within the electrochemical stability window of the used electrolyte.

Galvanostatic charge/discharge measurements were performed using a BTS 8.0 Battery Analyzer Neware 5 V 100 mA in a two-electrode configuration using glassy carbon as current collectors. Comparative charge/discharge curves were measured first at a common current density of 1 A g^{-1} for 5 cycles and afterward, at 5 A g^{-1} for 15,000 cycles with the upper cut-off voltage of 1.5 V. Based on these measurements, the specific capacitance of the electrode (C_s in F g^{-1}) was calculated according to Equation (1):

$$C_s = \frac{2(I\Delta t)}{Um} \quad (1)$$

with I / A being the discharge current, Δt / s discharge time, U / V the maximal voltage window and m / g the mass of the active material at a single electrode. The specific energy density of the constructed supercapacitor cells (E_s / Wh kg^{-1}) was calculated based on the mass of both electrodes (active materials) according to Equation (2):

$$E_s = \frac{1}{8} C_s U^2 \quad (2)$$

Electrochemical impedance measurements were performed on Gamry 1010E Potentiostat/Galvanostat in a previously described three-electrode configuration using a typical frequency interval of 10^{-2} to 10^5 Hz and AC voltage amplitude of 5 mV. For impedance measurements after the cycling stability test (5000, 10,000 and 15,000 cycles), the previously glavanostatically cycled electrodes were transferred to a three-electrode cell in a common electrolyte. The impedance spectra of both pristine and cycled electrodes were obtained at the fixed potential of 0.1 V corresponding to the redox process.

The complex impedance analysis was performed by applying Equations (3) to (5):

$$C(\omega) = -C_{re}(\omega) - jC_{im}(\omega) \quad (3)$$

$$C_{re}(\omega) = -Z''(\omega) / \omega |Z(\omega)|^2 \quad (4)$$

$$C_{im}(\omega) = -Z'(\omega) / \omega |Z(\omega)|^2 \quad (5)$$

$C_{re}(\omega)$ corresponds to the real part of the complex capacitance $C(\omega)$, in which a low-frequency value converges with the DC capacitance obtained by CV or galvanostatic measurements. $C_{im}(\omega)$, as an imaginary component of the complex capacitance $C(\omega)$, represents resistive losses that lead to energy dissipation.

All measurements were performed in 1 M $Al_2(SO_4)_3$, 1 M $Al(NO_3)_3$ and 1 M $AlCl_3$ electrolytes and at room temperature. Their electrical conductivity and pH were measured using Seven Compact pH/Conductometer S213 Mettler Toledo.

Results and discussion

ACvs700 microstructural characterization

Typical XRD of activated carbon, including reflections at 24 and 43° (2θ) indexed to (002) and (100) planes of graphite, is observed for ACvs700, Figure 1a. Broad and low-intensity diffraction peaks indicate its amorphous nature. The interplanar distance (002) estimated using Bragg's law amounts to 0.036704 nm, which aligns with the activated carbon structure [21]. SEM figure reveals irregular AC_{vs} micrometre agglomerates composed of nanoparticles embedded into deep holes formed during the liberation of gases during $ZnCl_2$-assisted activation. Material developed a high BET surface area of 1494 $m^2\ g^{-1}$ with high microporosity (Dubinin-Radushkevich method, V_{micro} = 0.548 $cm^3\ g^{-1}$) and meso-porosity fraction (Dollimore and Heal method V_{meso} = 0,254 $cm^3\ g^{-1}$).

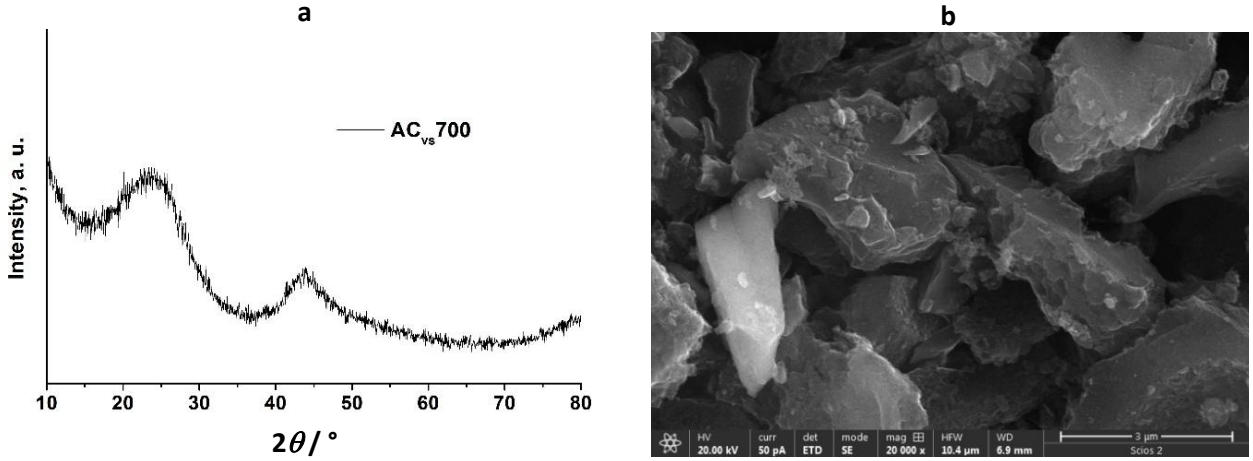

Figure 1. *XRD pattern a) and SEM image b) of AC_{vs}700*

Interfacial redox processes in Al-based electrolytes

Redox processes of AC_{vs}700 in 1 M Al-containing aqueous electrolytes ($Al_2(SO_4)_3$, $Al(NO_3)_3$ and $AlCl_3$) were characterized in a three-electrode configuration by CV at different scan rates (Figure 2 and Figure S1). Figure 2 shows the capacitive behaviour of AC_{vs}700 in all three electrolytes comparatively at a lower, medium, and higher scan rate. A similar current response was observed for all electrolytes at lower scan rates, Figure 2a. Due to their acidity, typical hydroquinone/quinone-related redox peaks observed at 0.15/0.08 V *vs.* SCE can be recognized [22,23]. Additionally, in $Al(NO_3)_3$, there is a deviation at negative potentials in the form of a small cathodic peak (-0.4 V vs. SCE), which appears before the hydrogen evolution reaction, belonging to the reduction of NO_3^- in an acidic medium [24]. As the scan rate increases (Figures 2b and 2c), the anion influence becomes more pronounced in the way that sulphates deviate from chlorides and nitrates.

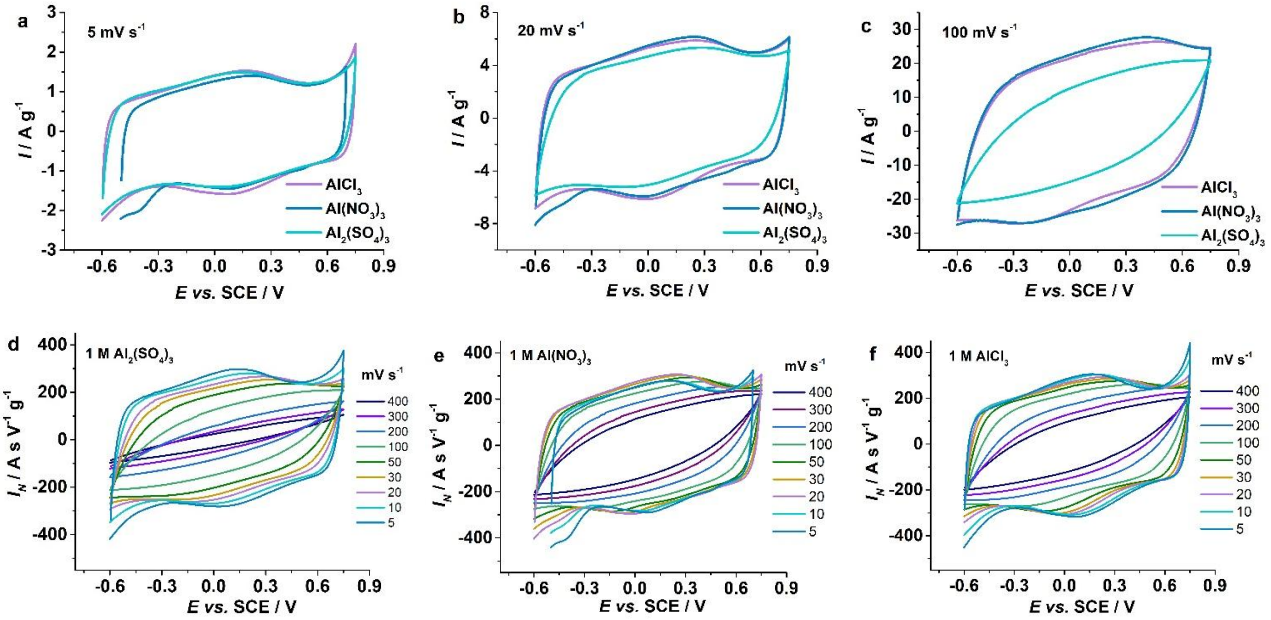

Figure 2. *Cyclic voltammograms of $AC_{vs}700$ in 1 M Al-based electrolytes at the scan rates of (a) 5 mV s^{-1}, (b) 20 mV s^{-1} and (c) 100 mV s^{-1} and (d), (e), (f) their scan rate-normalized form for at all scan rates*

To explain this behaviour, it is worth considering that $AC_{vs}700$ has a large specific surface area of S_{BET} = 1494 m^2 g^{-1}, relying on developed micro- (0.548 cm^3 g^{-1}) and mesoporosity (0.254 cm^3 g^{-1}), with wide micropore size distribution profile ≈0.5-0.7 nm (D_{max} = 0.5 nm) [13]. Namely, the correlation of these properties with the size of the used electrolyte ions could be beneficial. The differences in electrochemical behaviour of $AC_{vs}700$ in various Al-ion-based electrolytes can be explained by the larger hydrated radius of SO_4^{2-}, which causes their retarded adsorption and diffusion through the pores, while the smaller and similar radius of NO_3^- and Cl^- does not impede these processes as much [25,26]. Although the absolute radius of the hydrated specific (SO_4^{2-}, NO_3^- and Cl^-) anions is not consistent in literature (depending on the used approach and conditions taken into account) [25-27], the relation between their radii follows the same trend (SO_4^{2-} > NO_3^- > Cl^-). The micropores with a maximal diameter (0.5 nm) are less available for large SO_4^{2-} ions (the calculated diameter of solvated ions can reach values up to 0.533 nm [25]), which leads to a decrease in the number of ions that enter the total pores volume. Additionally, the measured electrical conductivity of $Al_2(SO_4)_3$ is more than four times lower than that of $AlCl_3$ and $Al(NO_3)_3$, resulting in slower movement of ions at higher scan rates, Table 1. A clear representation of this behavior is given by the scan rate-normalized CV graphs (Figure 1d, 1e and 1f), where it can be seen how, in $Al_2(SO_4)_3$, the voltammograms lose shape as the scan rate increases. On the other hand, in $AlCl_3$ and $Al(NO_3)_3$, these changes are much less pronounced.

Table 1. *Measured electrical conductivities and pH values of 1 M $Al_2(SO_4)_3$, $Al(NO_3)_3$ and $AlCl_3$.*

Electrolyte	1 M $Al_2(SO_4)_3$	1 M $Al(NO_3)_3$	1 M $AlCl_3$
Conductivity, mS cm^{-1}	25.733	104.751	114.199
pH	3.04	1.85	2.13

Comparative CV measurements implicate better rate capability in $AlCl_3$ and $Al(NO_3)_3$ while revealing the main obstacles for double layer formation in $Al_2(SO_4)_3$ electrolyte at extremely high currents. Still, their influence on the long-term stability of the material in a supercapacitor should be considered and examined in more detail.

To characterize the interface of pristine $AC_{vs}700$ electrode in 1 M $Al_2(SO_4)_3$, $Al(NO_3)_3$ and $AlCl_3$ (Figure 3a), Nyquist diagrams were measured at the potential of redox maxima. They show characteristic shapes of carbon electrodes. The high-frequency x-intercept typically belongs to the bulk electrolyte resistance, while the small semicircle, appearing in the high to mid-frequency range (10^6-38.11 Hz for $Al(NO_3)_3$, 10^6-139.2 Hz for $AlCl_3$ and 10^6- 5.197 Hz for $Al_2(SO_4)_3$, Figure 3a inset), corresponds to the interfacial impedance between electrode and bulk solution including the contact impedance between material and current collector, ion transport processes into pores, and charge transfer resistance (R_{ct}) [28,29]. Different diameters of the semicircle indicate the prevailing role of the kinetic hindrance effects in its appearance, determined by the type of electrolyte ions. The highest resistance value for $Al_2(SO_4)_3$ is governed by the lowest ionic conductivity, Table 1, and the highest hydration enthalpy of SO_4^{2-} anion [28]. There is no such correlation when it comes to $Al(NO_3)_3$ and $AlCl_3$, where the inversed behaviour was observed. A slightly larger high-frequency resistance point of $AlCl_3$ *vs.* $Al(NO_3)_3$ (despite better conductivity), as well as a somewhat smaller semicircle diameter (despite larger hydration enthalpy of Cl^- *vs*. NO_3^-), is probably the consequence of the poorer wettability of Cl^- *vs*. NO_3^- due to higher hydrophobicity [29]. The almost vertical region that prevails in the Nyquist diagram reflects a good pseudocapacitive behaviour of the material in all three types of electrolytes.

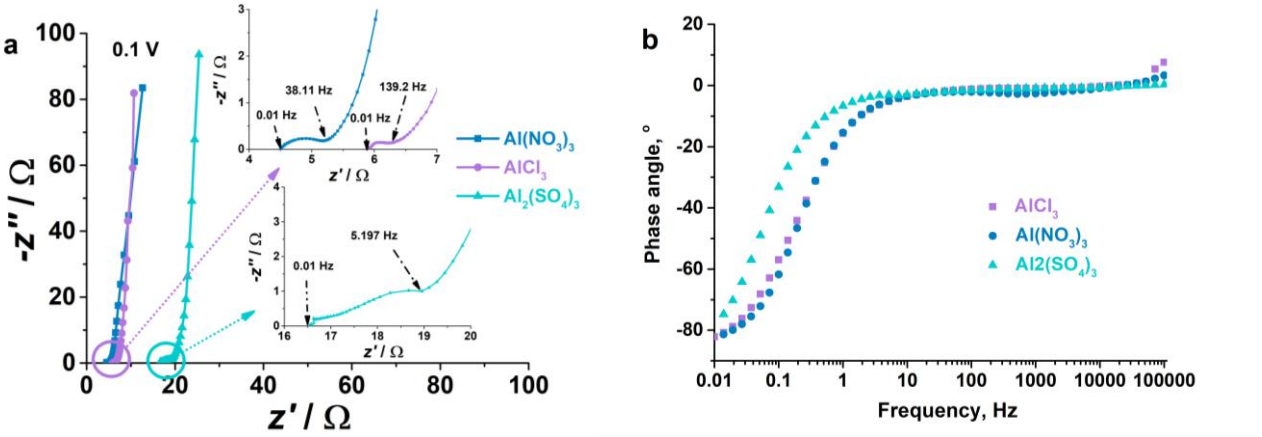

Figure 3. *Nyquist a) and Bode b) plots for $AC_{vs}700$ pristine in 1 M aqueous solutions of $Al_2(SO_4)_3$, $Al(NO_3)_3$ and $AlCl_3$ measured in a three-electrode cell. Inset shows enlarged high-frequency part of the Nyquist plot*

Dependence of the phase angle (φ) on the frequency (Figure 3b) indicates the almost ideal capacitor-like response with the low-frequency φ values very close to -90°, for all electrolytes. Dunn analysis of $AC_{vs}700$ in $Al_2(SO_4)_3$ [13] revealed that the electrical double layer capacitance (EDLC) dominates the total charge storage process (71 % at 5 mV s^{-1} and 83 % at 50 mV s^{-1}). Based on the phase angle-frequency dependence, this contribution is slightly higher for $AlCl_3$ and $Al(NO_3)_3$. The real and imaginary parts of the capacitance (Figure S2a and b) were obtained as a function of frequency by applying complex capacitance analysis. Figure S2a shows the characteristic real capacitance-frequency dependence with a high degree of ion pore-filling where the plateau is not fully achieved especially for the $Al_2(SO_4)_3$ electrolyte. Comparative capacitance values observed within the frequency region of 0.1 to 1 Hz follow the trend measured by CV at scan rates from 20 mV s^{-1}. There is a deviation in the low-frequency capacitance values (around 0.01 Hz) from those obtained by CV at lower scan rates (< 20 mV s^{-1}). This can be attributed to the nitrate-involved redox and water electrolysis reactions since the CV was measured over the extended voltage window, while the impedance diagrams were collected at a fixed potential corresponding to the CV maximum. The typical dependence of the imaginary capacitance part of the frequency, including the existence of the maximum at the frequency

f_0, was presented in Figure S2b. The time constant, $\tau_0 = 1/f_0$, when the system changed behaviour from the resistor to the capacitor one, was found to be around 9.9, 7.3 and 19.8 s for $AlCl_3$, $Al(NO_3)_3$ and $Al_2(SO_4)_3$, respectively. The time-constant trend in different electrolytes follows the corresponding changes of CV with the scan rate increase. The highest τ_0 for $Al_2(SO_4)_3$ indicates the most limited rate capability, which is in accordance with the large deviation of CV upon switching the scan rate to 400 mV s^{-1}, Figure S2b. A somewhat higher τ_0 value for $AlCl_3$ compared to $Al(NO_3)_3$ corresponds to a more pronounced CV deviation at high scan rates, Figure 2.

Exploring $AC_{vs}700$ charge storage ability in different Al-based full cells

To further investigate the stability of the material in the symmetric supercapacitor cell using all three Al-containing electrolytes, galvanostatic testing has been performed, Figure 4. The different shape of the charge/discharge curves in $Al_2(SO_4)_3$ and $AlCl_3$ compared to $Al(NO_3)_3$ indicates a different charge storage mechanism within the higher voltage range (1.2-1.5 V at 5 A g^{-1}), Figure 4a. In $Al(NO_3)_3$ electrolyte, the sloping part is evidenced within this range and diminishes with time. This can be attributed to the irreversible redox processes of NO_3^-, which are reduced in the vicinity of the positive electrode, thus oxidizing the carbon surface at higher voltages [19]. That contributes to significantly higher initial charge capacitance and slightly higher initial discharge capacitance for NO_3^- ions compared to $SO_4^{2-}$and Cl^-, resulting in low initial efficiency. No similar behaviour is observed for SO_4^{2-} and Cl^-.

The irreversibility of the NO_3^--involved process is responsible for the notable short-term capacitance fade in $Al(NO_3)_3$ at 5 A g^{-1} (Figure 4b), more pronounced at the lower current of 1 A g^{-1} (Figure S3), after which the capacitance becomes stable over 5000 cycles, with good efficiency. Stabilized capacitance values in $Al(NO_3)_3$ (≈75 F g^{-1} at 5000 cycles) are almost two times lower than in the other two electrolytes (130 F g^{-1} in $Al_2(SO_4)_3$ and 125 F g^{-1} in $AlCl_3$). The corresponding specific energy of the cell is also notably lower for $Al(NO_3)_3$ (5.8 Wh kg^{-1}) when compared to $Al_2(SO_4)_3$ and $AlCl_3$ (10.2 and 9.9 Wh kg^{-1}, respectively). Generated oxygen groups on the carbon surface at limiting potentials decrease specific surface area [30] and specific capacitance/energy. Therefore, $Al_2(SO_4)_3$ and $AlCl_3$ appear as more promising than $Al(NO_3)_3$. It can be seen that the carbon oxidation also occurs in $Al_2(SO_4)_3$ and $AlCl_3$ at lower current rates of 1 A g^{-1} (slightly more pronounced in $Al_2(SO_4)_3$), resulting in the difference between charge and discharge capacitance, Figure S3, but it does not significantly deteriorate its value upon cycling.

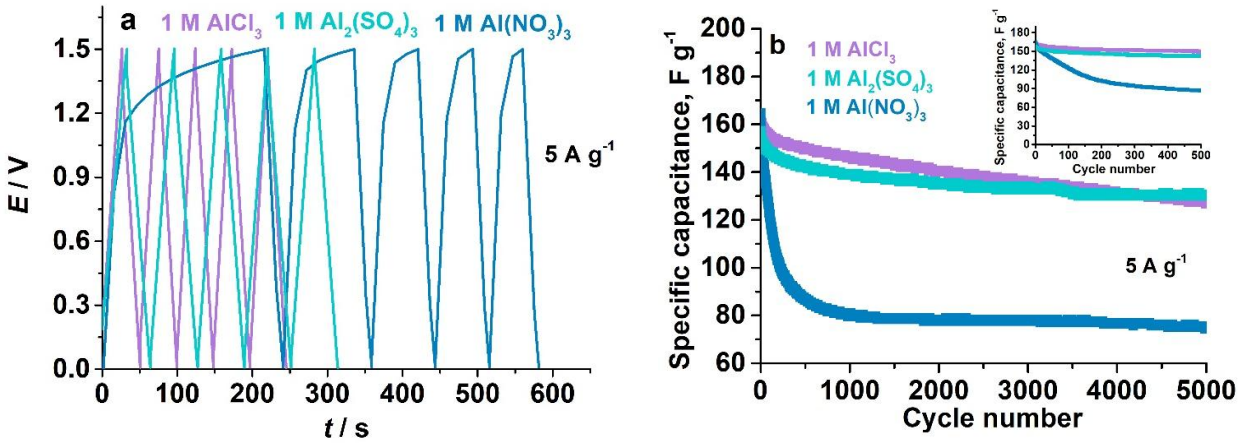

Figure 4. *$AC_{vs}700$-based supercapacitors with Al-ion containing electrolytes ($Al_2(SO_4)_3$, $Al(NO_3)_3$ and $AlCl_3$): (a) first five charge/discharge curves at 5 A g^{-1}, (b) specific capacitance vs. number of cycles for 5000 cycles at 5 A g^{-1}. Inset shows enlarged graph part within 0 to 500 cycles*

Unlike their Li analogues [18], the use of $Al(NO_3)_3$ does not offer an advantage over the other two Al-based electrolytes in terms of initial delivered energy. For both Li and Al aqueous salts, NO_3^--based electrolytes deteriorate the long-term stability of carbon (Fig 4b, inset).

The described galvanostatic behaviour from the two-electrode arrangement is reflected well through the impedance response of individual electrodes. Significant oxidation of the positive electrode in $Al(NO_3)_3$ over 5000 cycles responsible for the capacitance fade is evidenced through the appearance of the large semicircle, Figure 5a. Higher resistance values over the total frequency range measured in $Al(NO_3)_3$ also reflect the capacitance deterioration during cycling. The semicircle is not observed after cycling in $Al_2(SO_4)_3$ and $AlCl_3$, which correlates with good capacitance retention. Also, better wettability of the electrodes during charge/discharge can improve the transport of ions through pores and can result in depression of the initial semicircle measured before cycling. Since a certain degree of oxidation still occurs at the positive electrode at 1 A g^{-1} (the current density at which the cell was previously cycled) and is more pronounced for $Al_2(SO_4)_3$ than for $AlCl_3$, lower high-frequency intercept was observed for SO_4^{2-} containing electrolyte. Therefore, oxidation of the polarized positive electrode controls the high-frequency intercept by altering the wettability of the surface. The opposite effect was observed at a negative electrode, Figure 5b. Different processes at positive and negative electrodes are reflected in different phase angle-frequency profiles for specific electrolytes, Figures 5c and 5d. The peak-shaped phase angle response was measured for the positive electrode in $Al(NO_3)_3$ (after 5000 cycles) due to its strong oxidation (Figure 5c). This is a consequence of the aggravated penetration of ions through pores and their interaction with generated oxygen groups. This influence is not observed at the negative electrode, where the phase angle retains its characteristic initial shape (Figure 5d).

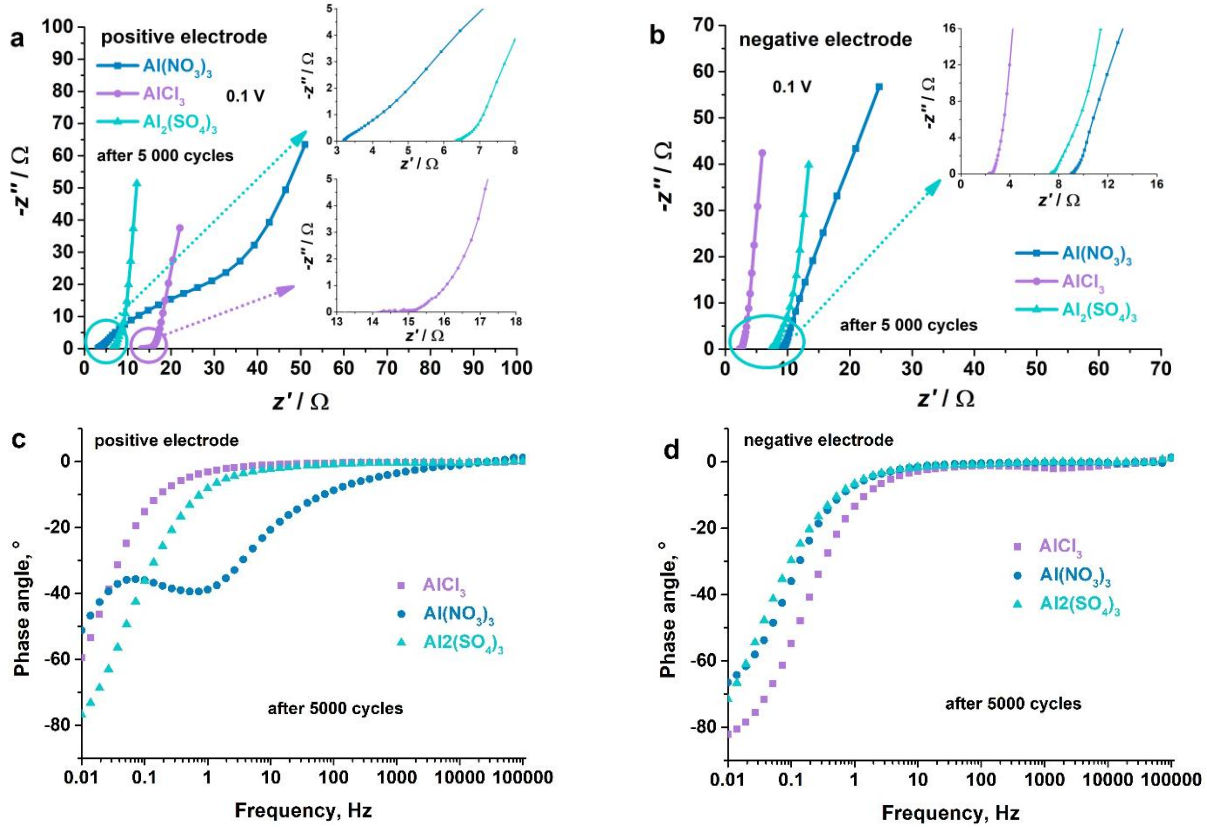

***Figure 5**. Nyquist (a, b) and Bode (c, d) plots for positive and negative $AC_{VS}700$ electrodes measured in a three-electrode cell after 5,000 cycles using 1 M aqueous solutions of $Al_2(SO_4)_3$, $Al(NO_3)_3$ and $AlCl_3$. Inset shows enlarged high-frequency part of the Nyquist plot*

To further observe if there are crucial differences between $Al_2(SO_4)_3$ and $AlCl_3$, the long-term stability test was performed over 15,000 cycles (Figure 6a). The notable difference is observed only after 10,000 cycles, where the capacitance in $AlCl_3$ starts to fade significantly and $Al_2(SO_4)_3$ keeps the same trend. The capacity retention of ACvs700/ACvs700 cells amounts to ≈83, ≈75 and ≈65 % in $Al_2(SO_4)_3$, while the corresponding values for $AlCl_3$ are ≈77, ≈67 and ≈30 % after 5,000, 10,000 and 15,000 cycles, respectively. Considering that the CV distortion in $Al_2(SO_4)_3$ starts after 20 mV s^{-1} (the current maximum corresponds to ≈ 5 A g^{-1}), excellent capacitance performance is still achieved at a current of 5 A g^{-1}.

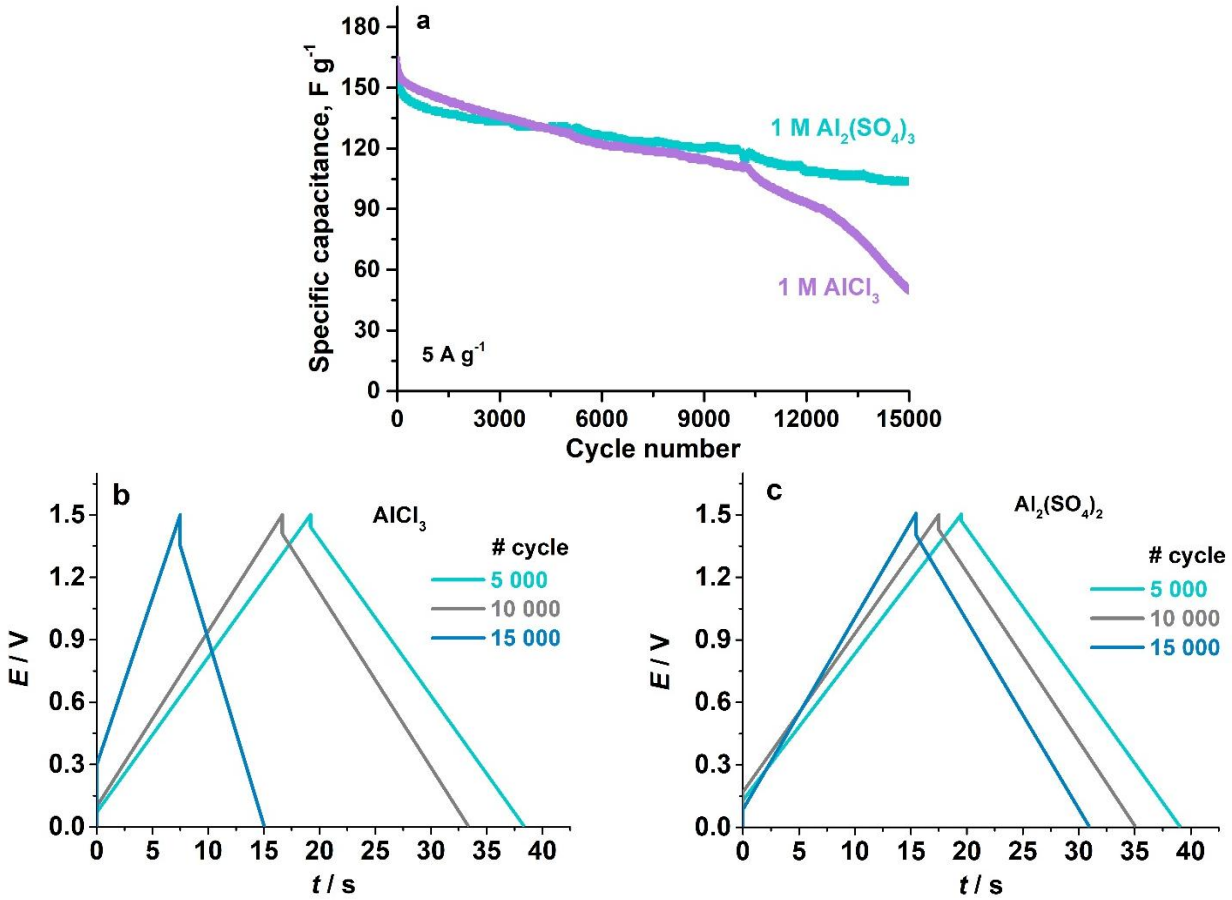

Figure 6. *a) Specific discharge capacitance* vs. *number of cycles $AC_{vs}700/AlCl_3/AC_{vs}700$ and $AC_{vs}700/Al_2(SO_4)_3/AC_{vs}700$ for 15000 cycles; b) charge/discharge curves of $AC_{vs}700/AlCl_3/AC_{vs}700$ and c) $AC_{vs}700/Al_2(SO_4)_3/AC_{vs}700$ at different cycles*

To summarize, $Al_2(SO_4)_3$ electrolyte delivered the best performance in terms of long-term stability, as evidenced also by the preservation of both charge/discharge (Figure 6c) and Nyquist curves of individual electrodes after 15,000 cycles (Figures 7c and d). On the other hand, these curves change in shape upon cycling ACvs700 in $AlCl_3$ after 10,000 cycles, in accordance with the decrease in capacitance. In the Nyquist plot, this is evidenced by the appearance of the large semicircle for the positive electrode (Figure 7a), which indicates more pronounced carbon oxidation during this cycling period. The oxidation also shifts the high-frequency intercept point to lower values (Figure 7a) and changes the shape of the phase angle-frequency profile, Figure 8a.

When the complex impedance analysis is applied, it can be seen that cycling limitations originate from the positive electrode ($C_{real}+ < C_{real}-$ and $\tau_o+ > \tau_o-$, Figure S4), especially after 15,000 cycles. All these effects are not observed in $Al_2(SO_4)_3$, thus confirming the low degree of oxidation during cycling within the potential window of 1.5 V and, consequently, good capacitance behaviour.

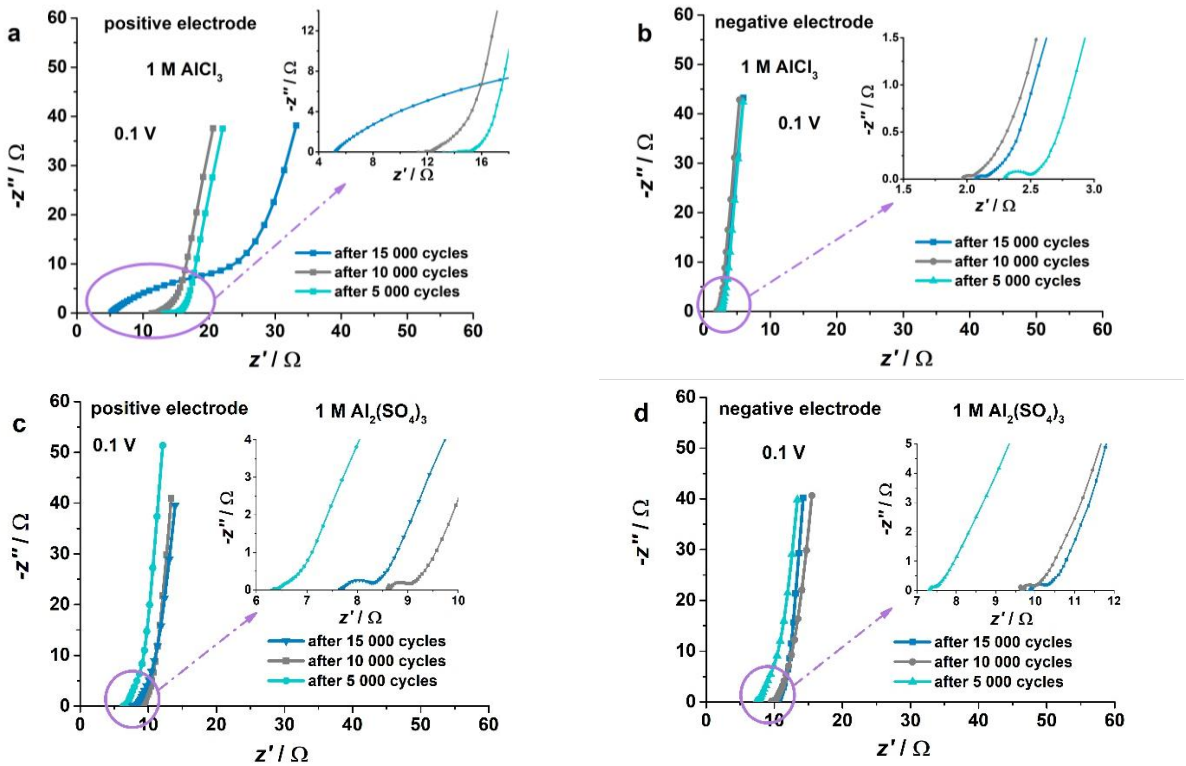

Figure 7. *Nyquist plots individual $AC_{vs}700$ electrodes measured in a three-electrode cell after 5,000, 10,000 and 15,000 cycles using 1 M aqueous solutions of $AlCl_3$ (a, b) and $Al_2(SO_4)_3$ (c, d). Inset shows enlarged high-frequency part of the Nyquist plot*

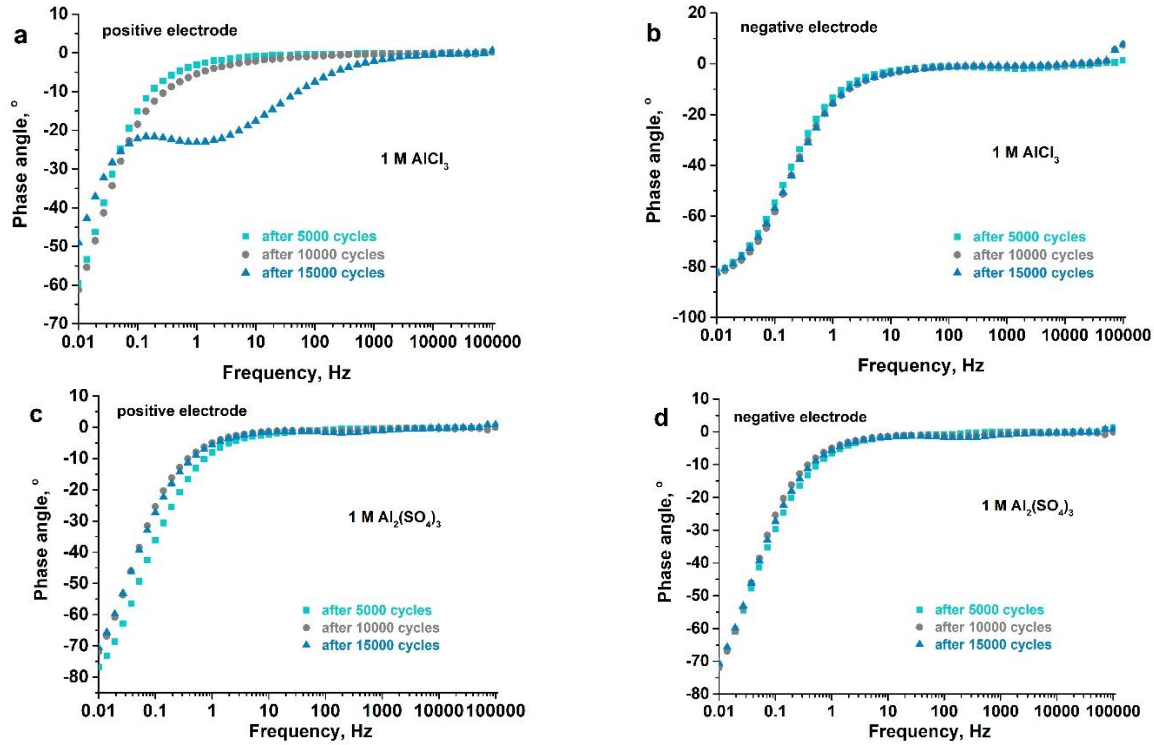

Figure 8. *Bode plots for positive and negative $AC_{vs}700$ electrodes measured in a three-electrode cell after 5,000, 10,000 and 15,000 cycles using 1 M aqueous solutions of $AlCl_3$ (a, b) and $Al_2(SO_4)_3$ (c, d)*

Conclusions

High-surface area vine shoots-derived activated carbon was examined as an electrode material in three Al-based aqueous electrolytes for non-conventional supercapacitors. Typical capacitance behaviour was observed in all examined electrolytes ($Al_2(SO_4)_3$, $Al(NO_3)_3$ and $AlCl_3$), while the type of

anion determines the rate capability and capacitance retention. Due to the larger size of SO_4^{2-} than NO_3^- and Cl^- ions, their penetration into pores is aggravated, which causes strong CV deviation at extremely high scan rates above 50 mV s^{-1}. This was not as pronounced for the other two salts, offering them an advantage. On the other hand, the presence of NO_3^- and Cl^- deterioration of the capacitance of 1.5 V ACvs700/ACvs700 cells at different levels of cycling depth. Due to the capability to be reduced in the proximity of the positive carbon electrode, NO_3^- progressively oxidizes its surface during initial cycling, thus causing the capacitance fade of the cell (up to ≈1000 cycles) to the stabilized value of ≈75 F g^{-1} after 5000 cycles. In $AlCl_3$, this oxidation process was delayed, thus producing significant capacitance fading only after 10,000 cycles (from ≈110 F g^{-1} after 10,000 cycles to ≈50 F g^{-1} after 15,000 cycles). In both $Al(NO_3)_3$ and $AlCl_3$, these processes can be evidenced through the appearance of the larger semicircle in the Nyquist diagram and the shifting of its high-frequency intercept point towards lower resistance values (better wettability due to *in-situ* generated oxygen groups). Pronounced oxidation is not observed for $Al_2(SO_4)_3$, as verified through the unchanged shape of charge/discharge and Nyquist curves throughout long-term cycling. As a result, carbon pores are more available for electrolyte ions, leading to higher capacitance values of the cell in $Al_2(SO_4)_3$ (≈131 F g^{-1} after 5,000 cycles) than in $Al(NO_3)_3$ (≈75 F g^{-1} after 5,000 cycles) and $AlCl_3$ (127 F g^{-1} after 5,000 cycles). Calculated energy density is also higher for $Al_2(SO_4)_3$ -based supercapacitor cell (10.2 Wh kg^{-1} after 5,000 cycles) than for $Al(NO_3)_3$- and $AlCl_3$-based supercapacitors (5.8 and 9.9 Wh kg^{-1} after 5,000 cycles, respectively). The best cyclic stability was observed in $Al_2(SO_4)_3$, demonstrated by relatively high values of ≈103 and 119 F g^{-1} after 10,000 and 15,000 cycles, respectively.

Supplementary material: *Additional data are available electronically on article page of the journal's website: https://pub.iapchem.org/ojs/index.php/JESE/article/view/2532, or from the corresponding author upon request.*

Acknowledgements: *This research was supported by NATO Science for Peace and Security (SPS) Programme under grant G5836-SUPERCAR. Authors gratefully acknowledge the financial support from the bilateral project Montenegro-Slovenia "Biomass-derived carbons as anodes in sodium-ion batteries". M. Vujković acknowledges the Ministry of Science, Technological Development and Innovation of the Republic of Serbia for support through the national programme (Contract number: 451-03-66/2024-03/200146).*

References

[1] D. Jiménez-Cordero, F. Heras, M. A. Gilarranz, E. Raymundo-Piñero, Grape seed carbons for studying the influence of texture on supercapacitor behaviour in aqueous electrolytes, *Carbon* **71** (2014) 127-138 https://doi.org/10.1016/j.carbon.2014.01.021.

[2] L. Guardia, L. Suárez, N. Querejeta, V. Vretenár, P. Kotrusz, V. Skákalová, T.A. Centeno, Biomass waste-carbon/reduced graphene oxide composite electrodes for enhanced supercapacitors, *Electrochimica Acta* **298** (2019) 910-917 https://doi.org/10.1016/j.electacta.2018.12.160.

[3] L. Alcaraz, A. Adán-Más, P. Arévalo-Cid, M. de F. Montemor, F. A. López, Activated Carbons From Winemaking Biowastes for Electrochemical Double-Layer Capacitors, *Frontiers in Chemistry* **8** (2020) 1-10 https://doi.org/10.3389/fchem.2020.00686.

[4] L. Suárez, T.A. Centeno, Unravelling the volumetric performance of activated carbons from biomass wastes in supercapacitors, *Journal of Power Sources* **448** (2020) 227413 https://doi.org/10.1016/j.jpowsour.2019.227413.

[5] J. Zhang, H. Chen, J. Bai, M. Xu, C. Luo, L. Yang, L. Bai, D. Wei, W. Wang, H. Yang, N-doped

hierarchically porous carbon derived from grape marcs for high-performance supercapacitors, *Journal of Alloys and Compounds* **854** (2021) 157207 https://doi.org/10.1016/j.jallcom.2020.157207.

[6] L. Guardia, L. Suárez, N. Querejeta, C. Pevida, T.A. Centeno, Winery wastes as precursors of sustainable porous carbons for environmental applications, *Journal of Cleaner Production* **193** (2018) 614-624 https://doi.org/10.1016/j.jclepro.2018.05.085.

[7] J. J. Manyà, B. González, M. Azuara, G. Arner, Ultra-microporous adsorbents prepared from vine shoots-derived biochar with high CO_2 uptake and CO_2/N_2 selectivity, *Chemical Engineering Journal* **345** (2018) 631-639 https://doi.org/10.1016/j.cej.2018.01.092.

[8] M. Erdem, R. Orhan, M. Şahin, E. Aydın, Preparation and Characterization of a Novel Activated Carbon from Vine Shoots by $ZnCl_2$ Activation and Investigation of Its Rifampicine Removal Capability, *Water, Air, & Soil Pollution* **227** (2016) https://doi.org/10.1007/s11270-016-2929-5.

[9] M. Ruiz-Fernández, M. Alexandre-Franco, C. Fernández-González, V. Gómez-Serrano, Adsorption isotherms of methylene blue in aqueous solution onto activated carbons developed from vine shoots (vitis vinifera) by physical and chemical methods, *Adsorption Science & Technology* **28** (2010) 751-759 https://doi.org/10.1260/0263-6174.28.8-9.751.

[10] B. Corcho-Corral, M. Olivares-Marín, E. Valdes-Sánchez, C. Fernández-González, A. Macías-García, V. Gómez-Serrano, Development of activated carbon using vine shoots (Vitis Vinifera) and its use for wine treatment, *Journal of Agricultural and Food Chemistry* **53** (2005) 644-650 https://doi.org/10.1021/jf048824d.

[11] J. A. S. B. Cardoso, B. Šljukić, M. Erdem, C. A. C. Sequeira, D. M. F. Santos, Vine shoots and grape stalks as carbon sources for hydrogen evolution reaction electrocatalyst supports, *Catalysts* **8** (2018) https://doi.org/10.3390/catal8020050.

[12] D. Alvira, D. Antorán, M. Vidal, V. Sebastian, Vine Shoots-Derived Hard Carbons as Anodes for Sodium- Ion Batteries: Role of Annealing Temperature in Regulating Their Structure and Morphology, *Batteries and Supercapacitors* **6** (2023) e202300233 https://doi.org/10.1002/batt.202300233.

[13] A. Gezović, J. Mišurović, B. Milovanović, M. Etinski, J. Krstić, V. Grudić, R. Dominko, S. Mentus, M.J. Vujković, High Al-ion storage of vine shoots-derived activated carbon New concept for affordable and sustainable supercapacitors, *Journal of Power Sources* **538** (2022) 231561 https://doi.org/10.1016/j.jpowsour.2022.231561.

[14] M. P. Bichat, E. Raymundo-Piñero, F. Béguin, High voltage supercapacitor built with seaweed carbons in neutral aqueous electrolyte, *Carbon* **48** (2010) 4351-4361 https://doi.org/10.1016/j.carbon.2010.07.049.

[15] L. Deng, G. Zhang, L. Kang, Z. Lei, C. Liu, Z.H. Liu, Graphene/VO_2 hybrid material for high performance electrochemical capacitor, *Electrochimica Acta* **112** (2013) 448-457 https://doi.org/10.1016/j.electacta.2013.08.158.

[16] L. Demarconnay, E. Raymundo-Piñero, F. Béguin, A symmetric carbon/carbon supercapacitor operating at 1.6 V by using a neutral aqueous solution, *Electrochemistry Communications* **12** (2010) 1275-1278 https://doi.org/10.1016/j.elecom.2010.06.036.

[17] K. Fic, G. Lota, M. Meller, E. Frackowiak, Novel insight into neutral medium as electrolyte for high-voltage supercapacitors, *Energy & Environmental Science* **5** (2012) 5842-5850 https://doi.org/10.1039/c1ee02262h.

[18] K. Fic, M. He, E.J. Berg, P. Novák, E. Frackowiak, Comparative operando study of degradation mechanisms in carbon-based electrochemical capacitors with Li_2SO_4 and $LiNO_3$ electrolytes, *Carbon* **120** (2017) 281-293 https://doi.org/10.1016/j.carbon.2017.05.061.

[19] J. Piwek, A. Platek, E. Frackowiak, K. Fic, Mechanisms of the performance fading of carbon-based electrochemical capacitors operating in a $LiNO_3$ electrolyte, *Journal of Power Sources*

438 (2019) 227029 https://doi.org/10.1016/j.jpowsour.2019.227029.
[20] J. Piwek, A. Platek-Mielczarek, E. Frackowiak, K. Fic, Enhancing capacitor lifetime by alternate constant polarization, *Journal of Power Sources* **506** (2021) 230131 https://doi.org/10.1016/j.jpowsour.2021.230131.
[21] J. M. V. Nabais, C. Laginhas, P. J. M. Carrott, M. M. L. R. Carrott, Thermal conversion of a novel biomass agricultural residue (vine shoots) into activated carbon using activation with CO_2, *Journal of Analytical and Applied Pyrolysis* **87** (2010) 8-13 https://doi.org/10.1016/j.jaap.2009.09.004.
[22] H. A. Andreas, B. E. Conway, Examination of the double-layer capacitance of an high specific-area C-cloth electrode as titrated from acidic to alkaline pHs, *Electrochimica Acta* **51** (2006) 6510-6520 https://doi.org/10.1016/j.electacta.2006.04.045.
[23] A. Śliwak, B. Grzyb, J. Ćwikła, G. Gryglewicz, Influence of wet oxidation of herringbone carbon nanofibers on the pseudocapacitance effect, *Carbon* **64** (2013) 324-333 https://doi.org/10.1016/j.carbon.2013.07.082.
[24] S. Garcia-Segura, M. Lanzarini-Lopes, K. Hristovski, P. Westerhoff, Electrocatalytic reduction of nitrate: Fundamentals to full-scale water treatment applications, *Applied Catalysis B: Environment and Energy* **236** (2018) 546-568 https://doi.org/10.1016/j.apcatb.2018.05.041.
[25] M. Endo, T. Maeda, T. Takeda, Y.J. Kim, K. Koshiba, H. Hara, M.S. Dresselhaus, Capacitance and Pore-Size Distribution in Aqueous and Nonaqueous Electrolytes Using Various Activated Carbon Electrodes, *Journal of The Electrochemical Society* **148** (2001) A910 https://doi.org/10.1149/1.1382589.
[26] H. Wu, X. Wang, L. Jiang, C. Wu, Q. Zhao, X. Liu, B. Hu, L. Yi, The effects of electrolyte on the supercapacitive performance of activated calcium carbide-derived carbon, *Journal of Power Sources* **226** (2013) 202-209 https://doi.org/10.1016/j.jpowsour.2012.11.014.
[27] Y. Marcus, Ionic radii in aqueous solutions, *Chemical Reviews* **88** (1989) 1475-1798 http://dx.doi.org/10.1021/cr00090a003.
[28] D. W. Smith, Ionic hydration enthalpies, *Journal of Chemical Education* **54** (1977) 540-542 https://doi.org/10.1021/ed054p540.
[29] X. Yang, Q. Xie, S. Yao, A comparative study on polyaniline degradation by an electrochemical quartz crystal impedance system: Electrode and solution effects, *Synthetic Metals* **143** (2004) 119-128 https://doi.org/10.1016/j.synthmet.2003.10.027.
[30] K. Fic, M. Meller, J. Menzel, E. Frackowiak, Around the thermodynamic limitations of supercapacitors operating in aqueous electrolytes, *Electrochimica Acta* **206** (2016) 496-503 https://doi.org/10.1016/j.electacta.2016.02.077.